HHS Public Access

Author manuscript

Nat Biomed Eng. Author manuscript; available in PMC 2020 January 28.

Published in final edited form as:

Nat Biomed Eng. 2020 January ; 4(1): 125–130. doi:10.1038/s41551-019-0357-8.

Adenine base editing in an adult mouse model of tyrosinemia

Chun-Qing Song[1,*], **Tingting Jiang**[1,*], **Michelle Richter**[2,3,4], **Luke H. Rhym**[5,11], **Luke W. Koblan**[2,3,4], **Maria Paz Zafra**[6], **Emma M Schatoff**[6,7], **Jordan L. Doman**[2,3,4], **Yueying Cao**[1], **Lukas E. Dow**[6], **Lihua Julie Zhu**[8,9,10], **Daniel G Anderson**[5,11], **David R. Liu**[2,3,4,#], **Hao Yin**[12,#], **Wen Xue**[1,8,10,13,#]

[1]RNA Therapeutics Institute, University of Massachusetts Medical School, Worcester, MA 01605, USA

[2]Department of Chemistry and Chemical Biology, Harvard University, Cambridge, Massachusetts 02138, USA.

[3]Howard Hughes Medical Institute, Harvard University, Cambridge, Massachusetts 02138, USA.

[4]Broad Institute of MIT and Harvard, Cambridge, Massachusetts 02141, USA.

[5]David H. Koch Institute for Integrative Cancer Research, Massachusetts Institute of Technology, Cambridge, Massachusetts, USA.

[6]Sandra and Edward Meyer Cancer Center, Department of Medicine, Weill Cornell Medicine, New York, New York, USA.

[7]Weill Cornell / Rockefeller / Sloan Kettering Tri-I MD-PhD program, New York, NY

[8]Department of Molecular, Cell and Cancer Biology, University of Massachusetts Medical School, Worcester, Massachusetts, USA.

[9]Program in Bioinformatics and Integrative Biology, University of Massachusetts Medical School, Worcester, Massachusetts, USA.

[10]Department of Molecular Medicine, University of Massachusetts Medical School, Worcester, Massachusetts, USA.

[11]Department of Chemical Engineering, Massachusetts Institute of Technology, Cambridge, Massachusetts, USA.

[12]Medical research institute, Wuhan university, Wuhan, PR China

[#]Communication can be sent to drliu@fas.harvard.edu, haoyin@whu.edu.cn, and Wen.Xue@umassmed.edu.
[*]These authors contributed equally to this work.

Author Contributions

CS, TJ, MR, DRL, HY, and WX designed the study. CS, TJ, MR, LHR, LWK, MPZ, EMS, JLD, YC, JZ, LED, and DGA performed experiments and analyzed data. CS, TJ, HY, and WX wrote the manuscript with comments from all authors.

Data availability

The authors declare that all data supporting the findings of this study are available within the paper and its Supplementary Information. The deep-sequencing data is available at the Sequence Read Archive under the accession code PRJNA513076.

Competing interests D.R.L. is a consultant and co-founder of Editas Medicine, Pairwise Plants, and Beam Therapeutics, which are companies that use genome editing. The other authors declare no competing interests.

[13]Li Weibo Institute for Rare Diseases Research, University of Massachusetts Medical School, 368 Plantation Street, Worcester, MA, 01605

Abstract

Unlike traditional CRISPR-Cas9 homology-directed repair, base editing can correct point mutations without supplying a DNA-repair template. Here, we show in a mouse model of tyrosinemia that hydrodynamic tail-vein injection of plasmid DNA encoding the adenine base editor (ABE) and a single guide RNA can correct an A>G splice-site mutation. ABE treatment partially restored splicing, generated fumarylacetoacetate hydrolase (Fah)-positive hepatocytes in the liver, and rescued weight loss in the animals. We also generated Fah+ hepatocytes in the liver via lipid-nanoparticle-mediated delivery of chemically modified sgRNA and an mRNA of a codon-optimized base editor that displayed higher base-editing efficiency than the standard ABE. Our findings suggest that adenosine base editing can be used for the correction of genetic disease in adult animals.

Point mutations are a frequent cause of genetic disease, with ~50% of disease point mutations being G:C>A:T [1]. CRISPR genome editing, dependent on double-stranded DNA breaks (DSB) followed by nonhomologous end-joining or homology-directed repair (HDR), has been applied to many organisms[2, 3]. However, major caveats of correcting point mutations through CRISPR genome editing include system efficiency, the introduction of DSBs and the need to provide DNA repair template. A new-generation of genome editing tool, Base Editing (BE) system, enables precise base changes (reviewed in [4, 5]), does not induce a high-level of DSBs, and finally does not require HDR donors for gene repair [4, 5].

To date, two classes of BEs have been developed [1, 6]. Cytosine BEs that include cytosine deaminases, Cas9 nickases, and uracil glycosylase inhibitor, introduces C•G to T•A base changes[6] and has been applied to successfully introduce a stop codon or correct T•A to C•G mutations in prokaryotes, fungi, plants, insects, amphibians, fish, and mammals [5, 7–11]. Adenine BEs comprise an evolved *Escherichia coli* TadA (ecTadA*, a tRNA adenosine deaminase evolved to accept DNA substrate) and Cas9 nickase, and mediate A•T to G•C substitutions[1]. Local delivery of ABE by intramuscular injection of trans-splicing AAV was recently reported[12]; however, systemic delivery of ABE for correction of liver disease in adult animals has not been investigated.

To explore the therapeutic potential of ABE in the liver of adult animals, we chose a mouse model of hereditary tyrosinemia type I (HTI), a fatal genetic disease. HTI is caused by loss-of-function of fumarylacetoacetate hydrolase (FAH), a key enzyme of the tyrosine catabolic pathway [13, 14]. FAH deficiency leads to accumulation of toxic metabolic intermediates, causing apoptosis of mutant hepatocytes and severe liver damage. The $Fah^{mut/mut}$ mouse model[14, 15] harbors a homozygous G•C to A•T point mutation in the last nucleotide of exon 8, resulting in exon skipping and loss of FAH protein. 2-(2-nitro-4-trifluoromethylbenzoyl)-1,3-cyclohexanedione (NTBC)[14] is an inhibitor of the tyrosine catabolic pathway upstream of FAH. $Fah^{mut/mut}$ mice need to be kept alive on NTBC-supplemented water to prevent toxin buildup and liver damage[14].

We and others recently reported that CRISPR can correct this Fah mutation through HDR[16–18] or allelic exchange[19]. Following correction by CRISPR, liver cells expressing the Fah enzyme, through their selective advantage, expand and repopulate the liver[14]. Thus, this mouse model is particularly suitable for testing ABE[13, 15].

Results

Use ABE to correct a *Fah* point mutation

The ABE editing window occupies positions ~4–9 with the 1st, 5' nucleotide (nt) of the candidate sgRNA counted as position 1 [1]. In order to edit the Fah mutation using ABE, we selected a previously validated Fah sgRNA [20] (Fig. 1a). The disease associated point mutation is located at position 9 (A9). This selected sgRNA is the only sgRNA position holding the necessary "NGG" PAM and targeting the mutation "A" within the ABE editing window. Notably, ABE-mediated editing at position A6 will change a serine codon into alanine (S235A), but this edit will not restore splicing. Initially, we tested different dosages of two ABE enzymes with different base editing windows[1], ABE6.3 and 7.10, in Fah mutant mouse embryonic fibroblast cells (MEF). Consistent with the literature[1], ABE6.3 resulted in the highest A>G base editing efficiency at position A9 (6.9 ± 2.0%,2 μg ABE6.3) (Supplementary Fig. 1) and editing efficiency was dependent of the ABE enzyme concentration. We therefore chose to test ABE6.3 in mice.

ABE generates Fah$^+$ hepatocytes in adult mouse liver

To deliver ABE to the liver of adult mice, we performed hydrodynamic tail vein injection[21] with ABE6.3 and our validated Fah sgRNA plasmids (named ABE thereafter, Fig. 1b). We removed NTBC-supplemented water 6 days after hydrodynamic injection to initiate HTI symptoms in Fah$^{mut/mut}$ mice. As shown in Fig. 1c, Fah$^{mut/mut}$ mice injected with control PBS or ABE6.3 alone rapidly lost 20% of total body weight. In contrast, ABE6.3 and FAH sgRNA rescued weight loss in all five mice (Fig.1c).

To examine whether ABE generates Fah$^+$ hepatocytes *in vivo*, we harvested three of the five mice at day 32 and stained liver sections with a Fah-specific antibody by immunohistochemistry (IHC). As shown in Fig. 1d and Supplementary Fig. 2, ABE generated widespread patches of Fah$^+$ hepatocytes in the Fah$^{mut/mut}$ livers due to the expansion of corrected hepatocytes[14]. Concordantly, ABE-treated mice showed improved liver histology compared to the liver damage in control Fah$^{mut/mut}$ mice off NTBC water (Fig. 1d and Supplementary Fig. 3). Consistent with published literature[14, 15], the rapid expansion of Fah$^+$ hepatocytes in the Fah$^{mut/mut}$ liver contributed to the rescue of weight loss in mice treated with ABE[14]. These data indicate that ABE rescues the Fah disease phenotype *in vivo*.

To determine whether ABE successfully corrects the HTI Fah splicing mutation in exon 8, we performed reverse transcription PCR (RT-PCR) in liver mRNA using primers spanning exon 5 and 9. As shown in Fig. 2a, we found that wild-type liver had a 405 bp PCR band containing exon 8 and Fah$^{mut/mut}$ liver had a 305 bp PCR band corresponding with truncated Fah mRNA lacking exon 8. In ABE-treated Fah$^{mut/mut}$ mice (post NTBC withdrawal and

hepatocyte expansion), we observed both 305 and 405 bp PCR bands, indicating that the exon 8 to exon 9 splicing was restored in a subset of hepatocytes. Sequencing of the 405 bp bands in ABE-treated mice confirmed the presence of the corrected "G" at position A9. (Fig. 2b). These data indicate that *in vivo delivery* of ABE corrects the G•C to T•A mutation in a subset of liver cells and generates the functional exon 8-containing Fah mRNA.

ABE partially corrects *Fah* mutation in the liver

To quantify ABE edited alleles post NTBC withdrawal, we amplified the Fah genomic region by PCR from liver DNA (using the same mice as in Fig. 1d), and performed amplicon deep sequencing. We observed that the A9 to G correction rate was 9.5±4.0%, ($n = 6$, Fig. 2c and Supplementary Table 1). Because many hepatocytes are 4N cells[20], it's possible that A9 in one allele was converted into G in the edited 4N hepatocytes.

Because position A6 of the Fah site is within the editing window of ABE (Fig. 1a), we also evaluated the editing efficiency at this position. We detected 1.9±0.9% A6 to G editing in livers (Fig. 2c). Compared to *in vitro* editing in MEFs (Supplementary Fig. 1), the *in vivo* detection of relatively lower A6G editing is likely due to re-population of A9G edited healthy cells in the liver rather than to an *in vivo* preference to A9 editing. The rate of both A6 to G and A9 to G editing (Fig. 2c) is low (~0.1%). Editing position A6 to G will change a serine codon into alanine (S235A) in the FAH enzyme. Because S235 is near the active site of the Fah enzyme[22], the A6G/A9G allele may compromise enzyme activity and impede functional rescue of edited hepatocytes.

We also measured the rate of insertions and deletions (indels) by deep sequencing. The detected indel rate was very low (0.05% ABE and 0.03% control) even after expansion of the edited hepatocytes (Fig. 2c and Supplementary Table 2). These data suggest that ABE can directly correct the Fah mutation without causing a high level of indel mutations. Two remaining ABE-treated mice were viable with normal body weight at 106 days without NTBC treatment (Fig. 2d and Supplementary Fig. 4), demonstrating the long-term viability and functionality of ABE treated hepatocytes.

Analysis of the off-target activity of ABE

To globally identify the off-target activity of ABE, we performed genome-wide Guide-Seq[23] *in vitro* followed by *in vivo* deep sequencing at selected off-target sites in mouse livers. First, we evaluated off-target activity *in vitro* using mouse Hepa1–6 cells stably expressing Cas9 and transfected with sgFah and Guide-Seq oligos[16]. Using the standard Guide-seq protocol, we detected only the *Fah* target site and one off-target site (defined as Guide-seq off-target site 1, or GOT1) (Supplementary Data Set 1). These data suggest that the Fah sgRNA used in this study is not associated with a large number of strong off-target sites. Next, we performed targeted deep sequencing *in vivo* in both control and ABE-treated livers. We did not detect increased A•T to G•C editing at GOT1 in ABE-treated livers compared to controls (n=4 mice, $p>0.05$) (Supplementary Fig. 5).

To expand our analysis, we sequenced four predicted top-ranking off-target sites in ABE-treated livers (n=6), and did not detect A•T to G•C editing above the background level in a control liver (all rates are <0.1%) (Supplementary Fig. 6). As the overall on-target ABE

efficiency in our *in vivo* study is relatively low, detecting off-target effects is difficult. Future work is needed to further study potential off-target editing of ABE [24, 25].

A codon-optimized RA6.3 improves ABE activity

New reports have indicated that efficiency of base editing can be improved with codon optimization of the Cas9 nickase and inclusion of an N-terminal nuclear localization sequence (NLS) [26, 27]. Optimized cytosine BEs and ABE7.10 have been reported [26, 27] but ABE6.3 has not been developed. To test if we could improve FAH base editing in our system, we cloned an optimized Cas9 nickase[26] into ABE6.3 (Fig. 3a) (named as reassembled ABE6.3 or RA6.3). When transiently transfected in cells, our optimized base editor, RA6.3, had substantially higher expression compared to ABE6.3 (Supplementary Fig. 7). To validate the efficiency of our optimized base editor, we transfected 293T cells with a selected sgRNA sequence with multiple "A" sites [1] to evaluate A•T to G•C substitution by position (Fig. 3b). Deep sequencing showed an increase in base editing efficiency at all adenine positions (including A9) with use of our codon optimized ABE RA6.3 (Fig. 3b).

To further confirm that RA6.3 improves editing efficiency, we compared the A-to-G conversion efficiency of ABE6.3 and RA6.3 at two other genomic sites in HEK293T cells (Fig. 4a, b). Our optimized RA6.3 increased A-to-G conversion rate at all the editable "A" sites within the editing window by an average of 2.1±0.9 fold (site1) and 4.8±1.8 fold (site2). Next, we compared the editing efficiency of HDR (100-nt single-stranded donor DNA) [1], ABE6.3 and RA6.3, at two genomic sites in HEK293T cells (Fig. 4c, d). Compared with HDR using short homologous arms (site1:1.7±1.1%; site2: 1.8±0.8%), ABE6.3 mediated substantially higher A•T to G•C conversion rates at targeted sites (site1: 30±6.3%; site2: 7.3±1.6%), while RA6.3 further increased base editing efficiency (site1: 61±6.3%; site2: 34±3.2%). These results confirm that the optimized ABE6.3 variant improves editing efficiency in cultured cells.

To compare RA6.3 and ABE6.3 *in vivo*, we measured the Fah editing efficiency following hydrodynamic injection of plasmids (Fig. 5a). IHC staining showed that RA6.3 generated more Fah-positive hepatocytes than ABE6.3 (Fig. 5b–c, $p<0.05$). This result was confirmed by deep sequencing of the *Fah* target site (Supplementary Fig. 8a). In addition, RA6.3 increased base editing at a second mouse genomic site *in vivo* compared to ABE6.3 (Supplementary Fig. 8b). Our combined *in vitro* and *in vivo* results indicate that RA6.3 is a robust base editor in mammalian cells and in the mouse liver.

LNP-mediated delivery of ABE mRNA and sgRNA *in vivo*

Finally, we used lipid nanoparticle (LNP) delivery[28] through tail vein injection to deliver our optimized RA6.3 mRNA with chemically-modified sgRNA (sgRNA) to the liver of adult mice (Supplementary Fig. 9a). To measure initial ABE efficiency, we kept the mice on NTBC water after i.v. injection to prevent hepatocyte proliferation. As shown in Supplementary Fig. 9b, $Fah^{mut/mut}$ mice injected with control PBS by IHC did not show any edited hepatocytes. In contrast, RA6.3 mRNA and FAH sgRNA showed 0.44% ± 0.28% edited hepatocytes (Supplementary Fig. 9c). The data suggest that non-viral delivery of ABE

is possible in the adult mouse liver and indicate the need to improve ABE mRNA stability and delivery vehicles.

Discussion

In summary, our results demonstrate that transient delivery of ABE and sgRNA by non-viral hydrodynamic injection is sufficient to generate Fah^+ hepatocytes and rescue the phenotypic weight loss of Fah mutant mice. We reported the first codon-optimized ABE6.3 and showed that *in vivo* delivery of ABE was able to correct the Fah mutation *in vivo* without inducing high-level indels. The relatively low rate of indel formation is one notable advantage of ABE-mediated gene correction compared to Cas9-mediated HDR. While we show phenotypic rescue in our FAH mice, the *in vivo* ABE efficacy in our proof-of-concept study may not suffice to treat other genetic disorders that require higher levels of correction and that do not selectively proliferate corrected cells. Thus, further improvement of ABE and delivery methods will continue to expand the utility of these powerful tools.

As an initial delivery vehicle, our study also showed that non-viral LNP delivery of ABE mRNA and sgRNA does generate FAH-positive hepatocytes *in vivo*, albeit with low efficiency. Because ABE mRNA is longer than Cas9 mRNA (5.2 kb vs 4.1 kb), it is possible that the delivery or translation of ABE mRNA is less efficient than Cas9 mRNA. Methods to improve delivery and to enhance mRNA stability/translation will be required to broaden the therapeutic application of ABE. This study demonstrates the potential application of ABE to correct disease genes with G•C to T•A point mutations in adult mammalian models.

METHODS

Construction of CRISPR vectors

sgRNA vector (U6_sgRNA_EFS_GFP, addgene #65656) expressing sgRNA[29] was digested with BsmBI. sgRNA Oligos were annealed, phosphorylated by T4 PNK, and ligated with linearized vector. RA6.3 vectors were cloned by Gibson assemble.

Mouse experiments

All animal study protocols were approved by the UMass IACUC. $Fah^{mut/mut}$ mice[14] were kept on 10mg/L NTBC water. Mice with more than 20% weight loss were humanely euthanized according to guidelines. Vectors for hydrodynamic tail vein injection were prepared using the EndoFreeMaxi Kit (Qiagen). For hydrodynamic liver injection, plasmids suspended in 2ml saline were injected via the tail vein in 5–7 seconds into 8–10 week old $Fah^{mut/mut}$ mice. The plasmid doses were: Figs. 1–2 30μg ABE plasmid + 60μg sgFah plasmid; Fig. 5 and Fig. S8a: 30μg ABE plasmid (or 30 μg RA6.3) + 30μg sgFah plasmid; Fig. S8b 30μg ABE plasmid (or 30 μg RA6.3) + 15μg sgAbc plasmid. The ABE RA6.3 mRNA was synthesized by TRILINK and end-modified sgRNA was synthesized by Axolabs (Kulmbach, Germany). Lipid nanoparticle formulation and treatment was recently published[28]. 1 mg/kg LNP RA6.3 mRNA and 0.5 mg/kg LNP Fah sgRNA were injected in 8–10 week old female $Fah^{mut/mut}$ mice via tail vein injection. The mice were injected 3–4 doses (every 3 days) and kept on NTBC water. Mice were harvested at 5 days post the last injection.

Immunohistochemistry

Mice were sacrificed by carbon dioxide asphyxiation. Livers were fixed with 4% paraformaldehyde (PFA), embedded in paraffin, sectioned at 5 μm and stained with hematoxylin and eosin (H&E) for pathology. Liver sections were de-waxed, rehydrated and stained using standard immunohistochemistry protocols[30]. The following antibody was used: anti-Fah (Abcam, 1:400). Representative images (of a total of >5 images) are shown.

Gene expression analysis and RT-PCR

RNA was purified using Trizol (Invitrogen) and reverse-transcribed using a High-Capacity cDNA Reverse Transcription Kit (Applied Biosystems). Full gel scans are shown in Supplementary Fig. 10.

Illumina sequencing

$Fah^{mut/mut}$ MEF cells were transformed by retroviral WZL-$HRas^{V12}$ and MSCV-shp53[31] to enhance transfection efficiency. ABE plasmids were electroporated into $Fah^{mut/mut}$ MEF. Genomic region was PCR amplified. Deep sequencing libraries were made from 1~100 ng of the PCR products. Libraries were normalized to approximately equal molar ratio, and sequenced on Illumina MiSeq machines (150bp, paired-end). Reads were mapped to the PCR amplicons as references using bwa with custom scripts (available in Supplementary Note 1 of ref. 1). Data processing was performed according to standard Illumina sequencing analysis procedures.

Comparison of ABE6.3, RA6.3 and HDR

HEK293T cells were seeded at a confluence of 60%. After 24h, cells were transfected with 1μg Cas9 or base editors, 300ng sgRNA expression plasmid, 6μl Lipofectamine 3000 (Thermo Fisher Scientific), and for HDR assays 0.7μg single-stranded donor DNA template (100nt, PAGE-purified from IDT) [1]. Genomic DNA was harvested 72h after transcription using quickextract buffer (Epicentre). Deep sequencing was performed to measure A to G conversion. Single-stranded 100-mer oligonucleotide donor templates and primers are listed in Table S3 and S4.

Guide-Seq

Deep-sequencing data from the GUIDE-seq experiment was analyzed using the GUIDEseq v1.10.0 Bioconductor Package[32] after barcode deconvolution, adaptor removal and alignment to mouse genome (mm10). The default settings for SpCas9 are used except that min.reads is set to 2 and min.peak. score.1strandOnly is set to 2 as in [33].

Supplementary Material

Refer to Web version on PubMed Central for supplementary material.

Acknowledgements

We thank C. Mello, P. Zamore, S. Wolfe, and E. Sontheimer for discussions and J. Smith for editing the manuscript. We thank Dr. Markus Grompe (Oregon Health & Science University) for providing the *Fah* mice. We thank Y. Liu and E. Kittler in the UMass Morphology and Deep Sequencing Cores for support. W.X. was supported by grants

from the National Institutes of Health (DP2HL137167, P01HL131471 and UG3HL147367), American Cancer Society (129056-RSG-16–093), the Lung Cancer Research Foundation, Hyundai Hope on Wheels, UMass CCTS, and ALS Association. This work was supported by DARPA HR0011–17-2–0049; U.S. NIH RM1 HG009490, R01 EB022376, U01 AI142756, and R35 GM118062; and HHMI (to D.R.L.), and R01 CA195787; K22 CA181280 (to L.E.D.). This work was supported in part by the Marble Center for Cancer Nanomedicine and a Cancer Center Support (core) Grant P30-CA14051 from the National Cancer Institute. M.R. was supported by the HHMI Hanna H. Gray Fellowship. L.W.K. is an NSF Graduate Research Fellow and was supported NIH Training Grant T32 GM095450. H.Y. was supported by the National Natural Science Foundation of China 31871345, the Young Thousand Talented Program from Wuhan University and the startup funding from Wuhan University.

References

1. Gaudelli NM et al. Programmable base editing of A*T to G*C in genomic DNA without DNA cleavage. Nature 551, 464–471 (2017). [PubMed: 29160308]
2. Cong L et al. Multiplex genome engineering using CRISPR/Cas systems. Science 339, 819–823 (2013). [PubMed: 23287718]
3. Mali P et al. RNA-guided human genome engineering via Cas9. Science 339, 823–826 (2013). [PubMed: 23287722]
4. Hess GT, Tycko J, Yao D & Bassik MC Methods and Applications of CRISPR-Mediated Base Editing in Eukaryotic Genomes. Molecular Cell 68, 26–43. [PubMed: 28985508]
5. Rees HA & Liu DR Base editing: precision chemistry on the genome and transcriptome of living cells. Nature Reviews Genetics (2018).
6. Komor AC, Kim YB, Packer MS, Zuris JA & Liu DR Programmable editing of a target base in genomic DNA without double-stranded DNA cleavage. Nature (2016).
7. Chadwick AC, Wang X & Musunuru K In Vivo Base Editing of PCSK9 (Proprotein Convertase Subtilisin/Kexin Type 9) as a Therapeutic Alternative to Genome Editing. Arteriosclerosis, thrombosis, and vascular biology 37, 1741–1747 (2017).
8. Kim K et al. Highly efficient RNA-guided base editing in mouse embryos. Nat Biotechnol 35, 435–437 (2017). [PubMed: 28244995]
9. Zong Y et al. Precise base editing in rice, wheat and maize with a Cas9-cytidine deaminase fusion. Nat Biotechnol 35, 438–440 (2017). [PubMed: 28244994]
10. Rossidis AC et al. In utero CRISPR-mediated therapeutic editing of metabolic genes. Nature Medicine 24, 1513–1518 (2018).
11. Villiger L et al. Treatment of a metabolic liver disease by in vivo genome base editing in adult mice. Nature Medicine 24, 1519–1525 (2018).
12. Ryu SM et al. Adenine base editing in mouse embryos and an adult mouse model of Duchenne muscular dystrophy. Nat Biotechnol (2017).
13. Azuma H et al. Robust expansion of human hepatocytes in Fah−/−/Rag2−/−/Il2rg−/− mice. Nat Biotechnol 25, 903–910 (2007). [PubMed: 17664939]
14. Paulk NK et al. Adeno-associated virus gene repair corrects a mouse model of hereditary tyrosinemia in vivo. Hepatology 51, 1200–1208 (2010). [PubMed: 20162619]
15. Aponte JL et al. Point mutations in the murine fumarylacetoacetate hydrolase gene: Animal models for the human genetic disorder hereditary tyrosinemia type 1. Proc Natl Acad Sci U S A 98, 641–645 (2001). [PubMed: 11209059]
16. Yin H et al. Therapeutic genome editing by combined viral and non-viral delivery of CRISPR system components in vivo. Nat Biotechnol 34, 328–333 (2016). [PubMed: 26829318]
17. Song CQ & Xue W CRISPR-Cas-related technologies in basic and translational liver research. Nat Rev Gastroenterol Hepatol 15, 251–252 (2018). [PubMed: 29443117]
18. Shao Y et al. Cas9-nickase-mediated genome editing corrects hereditary tyrosinemia in rats. J Biol Chem 293, 6883–6892 (2018). [PubMed: 29507093]
19. Wang D et al. Cas9-mediated allelic exchange repairs compound heterozygous recessive mutations in mice. Nat Biotechnol 36, 839–842 (2018). [PubMed: 30102296]
20. Yin H et al. Genome editing with Cas9 in adult mice corrects a disease mutation and phenotype. Nat Biotechnol 32, 551–553 (2014). [PubMed: 24681508]

21. Liu F, Song Y & Liu D Hydrodynamics-based transfection in animals by systemic administration of plasmid DNA. Gene Ther 6, 1258–1266 (1999). [PubMed: 10455434]
22. Bateman RL et al. Mechanistic inferences from the crystal structure of fumarylacetoacetate hydrolase with a bound phosphorus-based inhibitor. J Biol Chem 276, 15284–15291 (2001). [PubMed: 11154690]
23. Tsai SQ et al. GUIDE-seq enables genome-wide profiling of off-target cleavage by CRISPR-Cas nucleases. Nat Biotechnol 33, 187–197 (2015). [PubMed: 25513782]
24. Lee HK et al. Targeting fidelity of adenine and cytosine base editors in mouse embryos. Nature Communications 9, 4804 (2018).
25. Liang P et al. Genome-wide profiling of adenine base editor specificity by EndoV-seq. Nature Communications 10, 67 (2019).
26. Zafra MP et al. Optimized base editors enable efficient editing in cells, organoids and mice. Nat Biotechnol (2018).
27. Koblan LW et al. Improving cytidine and adenine base editors by expression optimization and ancestral reconstruction. Nat Biotechnol (2018).
28. Yin H et al. Structure-guided chemical modification of guide RNA enables potent non-viral in vivo genome editing. Nature Biotechnology (2017).
29. Hsu PD et al. DNA targeting specificity of RNA-guided Cas9 nucleases. Nat Biotechnol 31, 827–832 (2013). [PubMed: 23873081]
30. Xue W et al. Response and Resistance to NF-kappaB Inhibitors in Mouse Models of Lung Adenocarcinoma. Cancer Discov 1, 236–247 (2011). [PubMed: 21874163]
31. Xue W et al. Senescence and tumour clearance is triggered by p53 restoration in murine liver carcinomas. Nature 445, 656–660 (2007). [PubMed: 17251933]
32. Zhu LJ. et al. GUIDEseq: a bioconductor package to analyze GUIDE-Seq datasets for CRISPR-Cas nucleases.
33. Yin H et al. Partial DNA-guided Cas9 enables genome editing with reduced off-target activity. Nat Chem Biol 14, 311–316 (2018). [PubMed: 29377001]

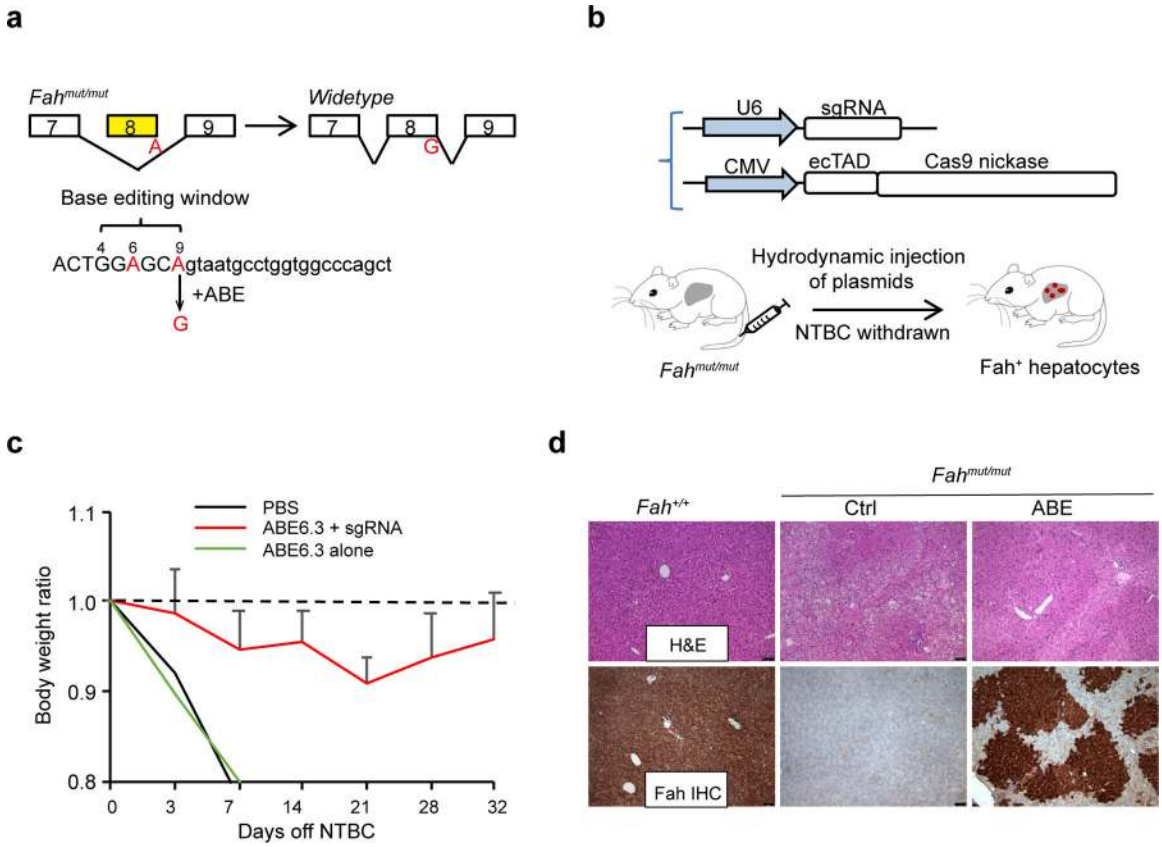

Figure 1. ABE rescues liver disease phenotype in a mouse model of tyrosinemia.

(A) Fah$^{mut/mut}$ mice harbor a G>A mutation (red) at the last nucleotide of exon 8, causing exon skipping. Exon sequences are in upper case. G>A mutation is at position 9 of the sgRNA target. (B) Hydrodynamic injection of ABE and sgRNA plasmids. (C) ABE6.3+sgRNA rescues body weight loss. Withdrawal of NTBC water is defined as Day 0. Error bars indicate s.d. (n=5 mice). In the ABE6.3+sgRNA group, the final body weight is significantly different from the lowest weight (P=0.02, one-tailed student t test). (D) ABE-treated mice show regions of Fah+ hepatocytes (n=3 mice, 32 days off NTBC). Scale bars = 75 μm.

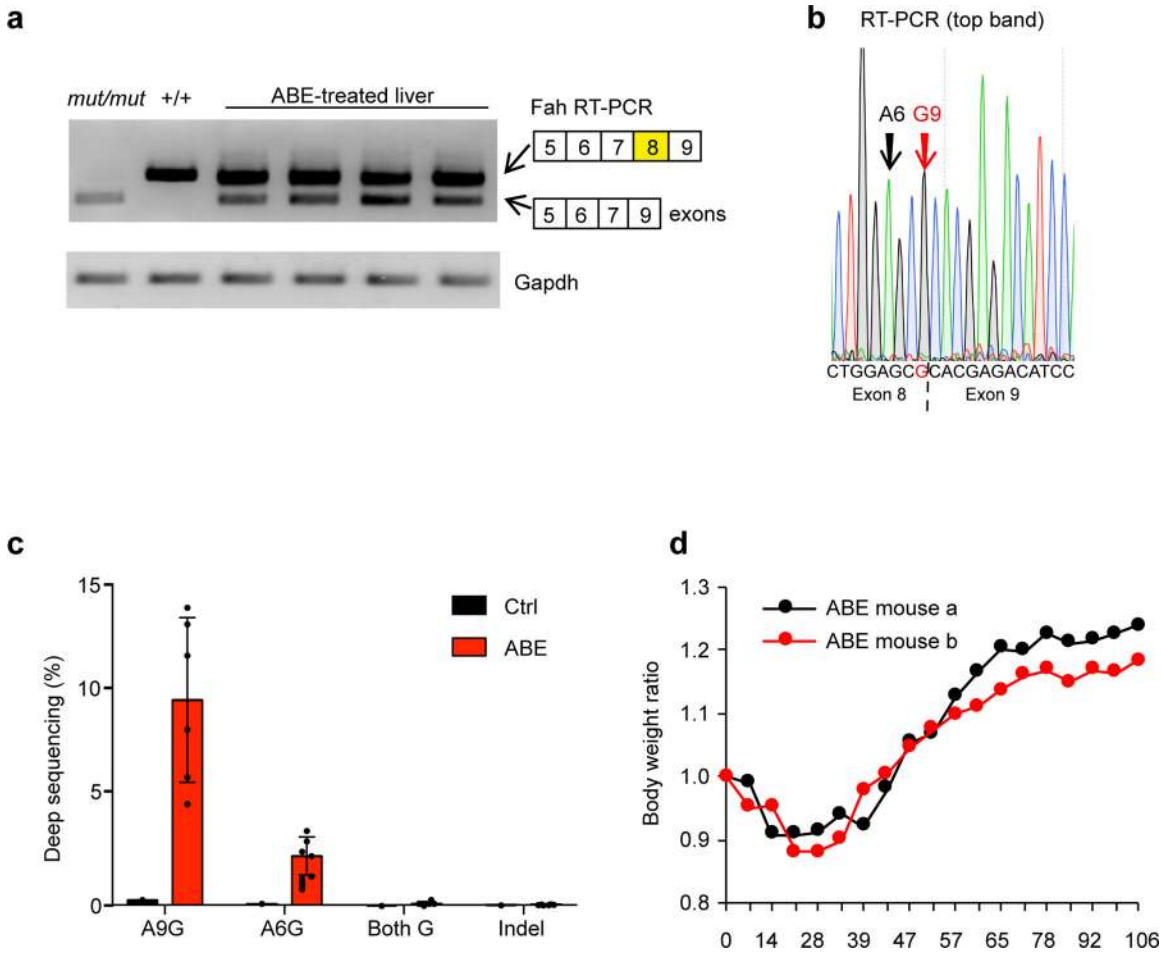

Figure 2. ABE partially corrects the Fah mutation in mouse liver.

(A) RT-PCR in a representative ABE mouse (4 liver lobes) using primers spanning exon 5 and 9. Wildtype Fah (+/+) amplicon is 405bp and mutant Fah (lacking exon 8) is 305bp. Gapdh, control gene. Images of the uncropped gels are provided in Supplementary Fig. 10. (B) Representative Sanger sequencing of the 405bp RT-PCR bands. (C) Deep sequencing of Fah genomic region in liver DNA. Error bars are s.d. (n=6 liver samples from two mice). (D) Long-term survival of two ABE-treated mice (a and b) without NTBC.

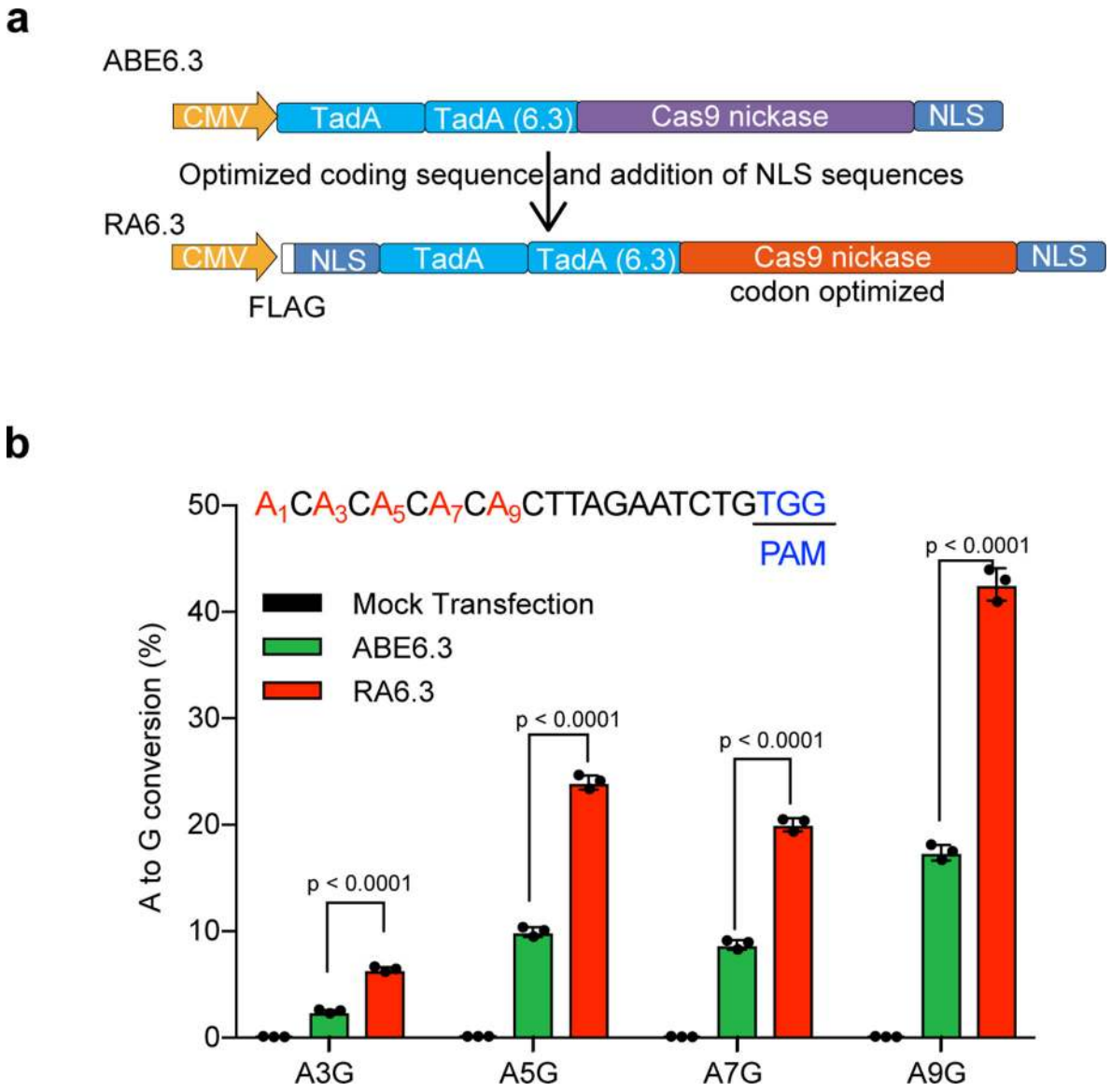

Figure 3. Optimizing the coding sequence of ABE6.3 and adding N-terminal NLS sequences improves base editing.

(a) Schematic representation of codon-optimized ABE 6.3. (b) Frequency of A-to-G editing in HEK293T cells 5 days after ABE and sgRNA transfection. Graphs show mean values. Error bars indicate s.d. (n = 3 biologically independent samples). P values determined by one-tailed student t tests.

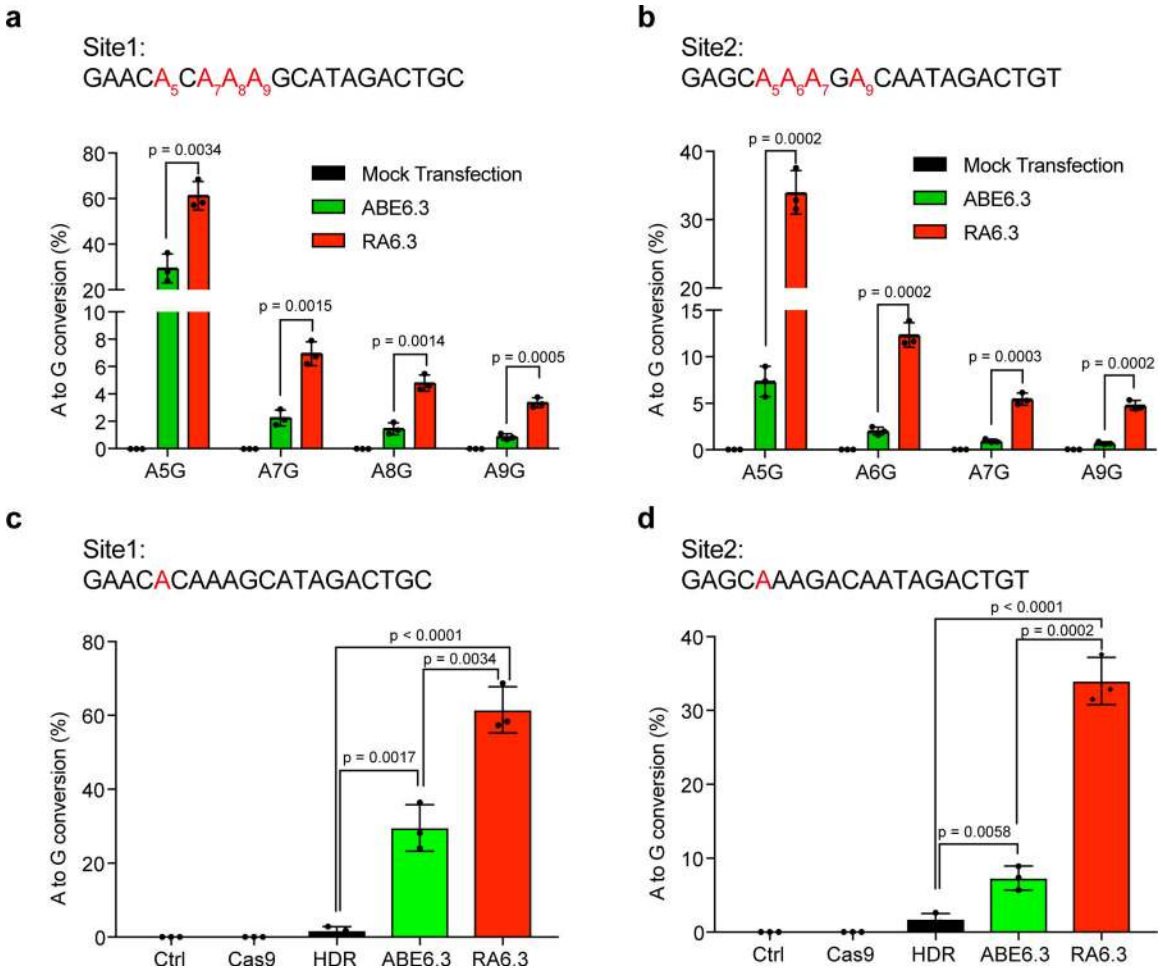

Figure 4. RA6.3 shows a higher editing efficiency compared to ABE6.3 and Cas9-mediated HDR at two genomic sites in HEK293T cells.

(a,b) Frequency of A-to-G editing at different positions at two genomic sites (sequences as indicated). The "A"s within the editing window are in red. (c,d) Frequency of A-to-G conversion at a targeted A (in red) mediated by ABE6.3, RA6.3 or HDR at two genomic sites (sequences as indicated). Cas9 indicates the group transfected with Cas9 plasmid alone. All error bars indicate s.d. (n = 3 biologically independent samples). P values determined by one-tailed student t tests.

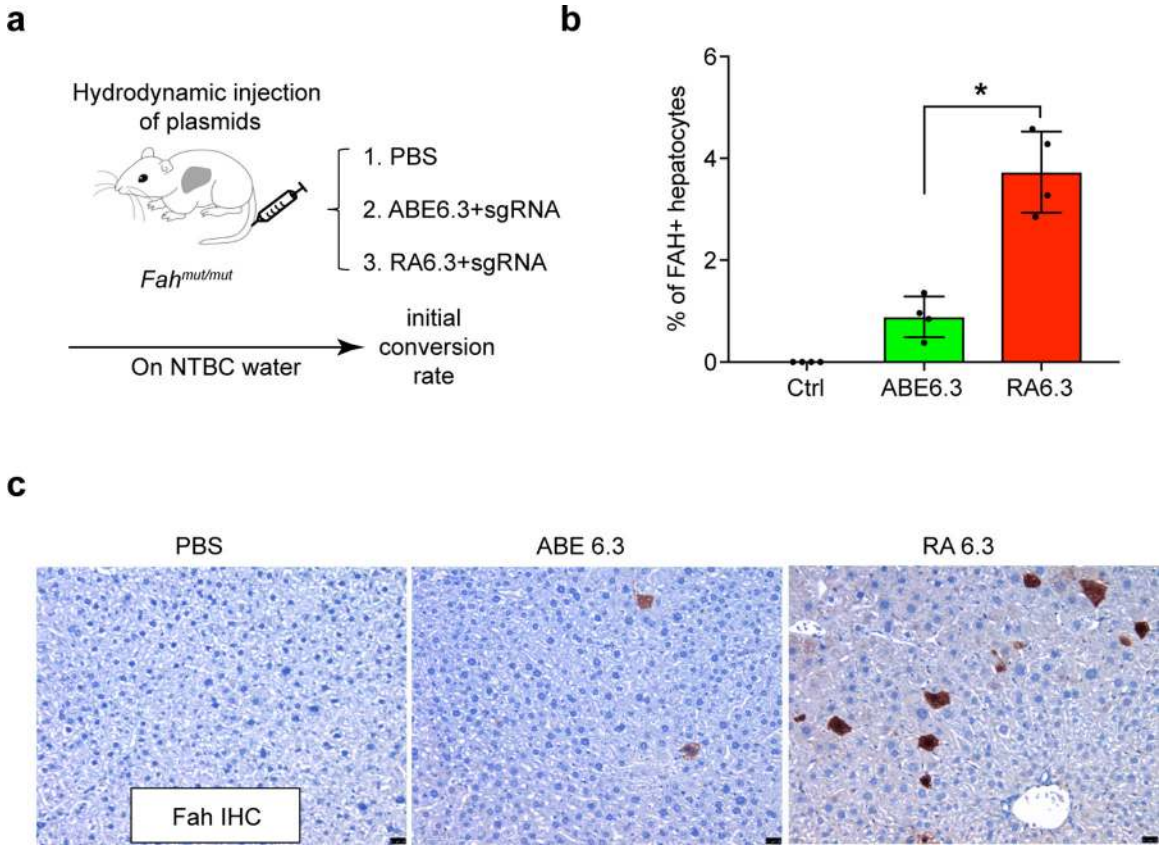

Figure 5. RA6.3 increases editing efficiency in vivo compared to ABE6.3.

(a) *Fah*$^{mut/mut}$ mice were injected with indicated plasmid combinations. To measure initial A->G conversion rate, mice were kept on NTBC to prevent expansion of corrected cells. (b) Quantification of Fah-positive hepatocytes by IHC at day 7. Error bars indicate s.d. (n=4 mice per group). *P = 0.0143 by one-tailed Mann-Whitney test. (c) Representative Fah IHC. Scale bars are 25um.